Aalborg Universitet

AALBORG UNIVERSITY
DENMARK

A sensorless active control approach to mitigate fatigue loads arising from the torsional and blade edgewise vibrations in PMSG-based wind turbine system

Safaeinejad, Ali; Rahimi, Mohsen; Zhou, Dao; Blaabjerg, Frede

Published in:
International Journal of Electrical Power & Energy Systems

DOI (link to publication from Publisher):
10.1016/j.ijepes.2023.109525

Publication date:
2024

Link to publication from Aalborg University

Citation for published version (APA):
Safaeinejad, A., Rahimi, M., Zhou, D., & Blaabjerg, F. (2024). A sensorless active control approach to mitigate fatigue loads arising from the torsional and blade edgewise vibrations in PMSG-based wind turbine system. *International Journal of Electrical Power & Energy Systems*, *155*(Part A), 1-20. Article 109525. https://doi.org/10.1016/j.ijepes.2023.109525

General rights
Copyright and moral rights for the publications made accessible in the public portal are retained by the authors and/or other copyright owners and it is a condition of accessing publications that users recognise and abide by the legal requirements associated with these rights.

- Users may download and print one copy of any publication from the public portal for the purpose of private study or research.
- You may not further distribute the material or use it for any profit-making activity or commercial gain
- You may freely distribute the URL identifying the publication in the public portal -

Take down policy
If you believe that this document breaches copyright please contact us at vbn@aub.aau.dk providing details, and we will remove access to the work immediately and investigate your claim.

A sensorless active control approach to mitigate fatigue loads arising from the torsional and blade edgewise vibrations in PMSG-based wind turbine system

Ali Safaeinejad [1], Mohsen Rahimi [2*], Dao Zhou[3], Frede Blaabjerg[4]

1,2 Department of Electrical and Computer Engineering, University of Kashan, Kashan, Iran

3,4 Department of Energy Technology, Aalborg University, Aalborg DK-9220, Denmark

[1]a.safaeinejad@grad.kashanu.ac.ir

[2]*mrahimi@kashanu.ac.ir

[3]zda@energy.aau.dk

[4]fbl@energy.aau.dk

Abstract

Fatigue loads associated with torsional and blade-edgewise vibrations are recognized as major reasons of large scale wind turbine failures. This paper presents an active mitigating control approach to reduce torsional and edgewise vibrations in the PMSG-based wind turbine. Due to the interactions of both vibrations, the active control is designed based on the expanded dynamic model of the mechanical-structural flexibilities. In this way, the blades are modeled as flexible cantilever beams, and thus, in the drive-train model the dynamics of the blades are considered. The control input to suppress the vibrations is achieved by the power electronic converters through adding an axillary term proportional to the speed difference between the blade and hub into the power control loop. This term manipulates the generator torque to counteract the unwanted vibrations. The needed drive-train and mechanical variables for making the auxiliary term are estimated by a novel robust method based on the sliding-mode observer. Using mathematical analyses and simulation results, it is shown that the proposed active mitigating approach well alleviates the fatigue loads of the torsional and edgewise modes even under severe changes in the drive-train stiffness coefficients. Thus, the proposed sensorless control approach is an appropriate remedy action for alleviation of WT fatigue loads even under parameters uncertainties.

Keywords: Torsional oscillations, edgewise vibrations, PMSG-based WT, active mitigating control, power control loop, parametric uncertainty

1. Introduction

Nowadays wind power plants are known as a mature technology among the industries of renewable energies and have experienced considerable developments in the size of structural components of the wind turbines [1]. These structures are usually manufactured from lightweight and high-strength materials which have flexible and lightly damped properties. On the other hand, as the capacity of a wind turbine (WT) increases, the transmitted forces and torques on the blades and drive-train components become larger. This means that they become more vulnerable to external dynamic excitations such as aerodynamic and electric disturbances [2]. These disturbances are constantly imposed on the large scale WTs during their entire service life which can cause fatigue, failure and deformation in the blades and drive-train components [3]. From the reliability issue

point of view, the blade fragments and drive-train components, as the costly structures of the WTs, have the major contribution to the overall failure rates and downtimes, and thus the blades and drive-train components are responsible for a considerable quota of the maintenance costs [4].

Drive-train fatigues known as torsional oscillations are caused by speed difference between the rotor and the generator [5-8]. Blade fatigues are recognized as flapwise vibrations and edgewise vibrations. Flapwise vibrations occur in perpendicular to the rotor rotational plane whereas edgewise vibrations occur along the rotational plane. The edgewise vibrations arise from the fluctuations of the aerodynamic torque and output power, in which aerodynamic damping is very low in comparison with flapewise vibrations [2, 9-11]. As a result, the weak damped torsional oscillations can impress on the edgewise vibrations. Hence, both torsional and edgewise fatigues are among the main challenges in operating of a large scale WT. In order to preserve the structural safety in the WTs, it is imperative to investigate the torsional and edgewise vibrations and study appropriate fatigue mitigating strategies [10]. Hence, it is essential understanding the dynamic interaction between the mechanical, structural and electrical systems of the WTs [12].

Fatigue mitigating methods in general can be classified as passive and active method. A passive mitigating method needs additional devices mounted on the WT structures and does not exert any force into the system and exclusively dissipates the oscillatory energy, thus creating costs and restrictions for the WT. Active mitigating methods with using the energy achieved by the control system counteract the harmful vibrations and are more efficient than the passive methods [3, 10]. There is now increasing interest in employing the active mitigating approaches for reduction the mechanical-structural loading of the WTs.

To the best knowledge of the authors, any comprehensive research on active mitigating of both torsional and edgewise vibrations considering the interaction between the structural, mechanical and electrical parts has not been reported in the literature. In [13], the dynamic interaction of electrical and structural components for a DFIG-based WT is investigated, and then the influence of grid disturbances on the edgewise vibrations is shown. However, this paper has not considered any control scheme to improve these vibrations, moreover the impact of aerodynamic changes on the edgewise vibrations has not been addressed. In [14, 15] first, the mathematical model to describe the dynamic behavior of the edgewise vibrations is presented, and then an active mitigating approach is designed to suppress the edgewise loading. The active control proposed in these papers uses special sensors and actuators embedded inside the each blade, thus bringing up extra costs and reducing the WT reliability.

There is extensive research dealing with the active mitigating of the torsional oscillations. In classic approaches, an auxiliary damping torque is built by feeding the generator speed measurement through a band-pass filter or a low-pass filter tuned around the dominant drive-train eigenfrequency [16-19]. Due to dependency of the discussed methods on filters parameters, the efficacy of them can be compromised when subjected to parametric uncertainties. To overcome this shortcoming, in Refs. [5-8] for the DFIG and PMSG WTs the auxiliary damping torque is realized by taking the speed deference between the low-speed and high-speed shafts, where in [7, 8], the PMSG-WT operates in the speed control mode.

Due to instinct advantages of permanent magnet synchronous generators (PMSGs) for multi-megawatts applications [20], this work is carried out on a PMSG-based WT. Figure 1 shows the grid-tied PMSG-based WT via power electronic converters, known as machine-side converter (MSC) and grid-side converter (GSC). In this paper, the control strategy for power electronic converters is established based on the power control mode which is in agreement with practical cases [21]. This paper proposes robust active mitigating approach considering both blade edgewise vibrations and drive-train torsional oscillations. The proposed control approach is performed with creating an auxiliary damping torque based on the difference between the blade and hub speeds. The novelty and contributions of this paper are as follows: 1) Extraction the detailed modeling of the WT system focusing on the interaction between the electrical, mechanical and structural parts , 2) Identifying the oscillatory modes associated with the torsional and mechanical flexibilities, 3) Proposing an active mitigating approach for reducing the mechanical-structural vibrations, and 4) Robust estimation the required variables for providing the auxiliary damping term as a novel sensorless method based on sliding mode observer (SMO)

The organization of this paper is as follows: Section 2 presents the dynamic modeling of the grid-tied PMSG-based WT. Small signal and modal analysis for the WT with original control loops are carried out in section 3. In section 4 the proposed active mitigating approach is introduced and its performance is verified by using the modal analysis. Designing the sensorless SMO-based estimator for realizing the proposed active mitigating approach is presented in section 5. Further, the simulation results under several test cases are given in section 6.

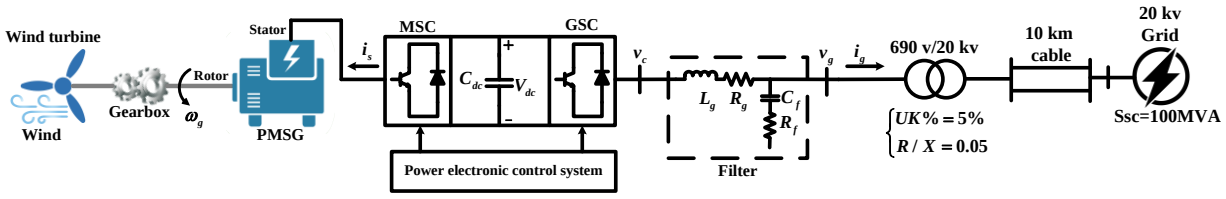

Fig. 1. Schematic diagram of the study grid-tied PMSG based WT

2. Modeling of the grid-tied PMSG-based WT

In this section, dynamic modeling of the PMSG-WT comprising aerodynamic, mechanical-structural, generator and control subsystems, is presented.

2.1. Aerodynamic system

For a horizontal axis 3-bladed wind turbine with considering blade passing phenomenon (BPPh), the turbine torque captured in the aerodynamic conversion process can be written as [22-25]:

$$T_t = T_m + \tilde{T}_{BP} \tag{1}$$

$$T_m = \frac{1}{2}\rho\pi R^2 (V_w - x_{nd}^{\cdot})^3 C_p(\lambda,\beta)/\omega_b \tag{2}$$

$$\tilde{T}_{BP} = \frac{2}{mV_H}\left[v_{eq_{ws}} + v_{eq_{ts}} + (1-m)V_H\right]T_m \tag{3}$$

where T_m is the average value of the turbine torque and $\tilde{T}_{BP}$ is the oscillatory component of the turbine torque associated with BPPh. Also, ρ, R, V_w, $x_{nd}^{\cdot}$ and ω_b are the air density, length of blades, spatial average wind speed, displacement speed of the tower top and rotational speed of the blades, respectively. C_p is defined as the power coefficient of the blades related to the WT specifications and is a function of the tip speed ratio, λ, and blade pitch angle, β, and λ as the tip speed ratio, is given by

$$\lambda = \frac{R\omega_b}{(V_w - x_{nd}^{\cdot})} \tag{4}$$

Further, m is relevant to the proportional ratio between spatial wind speed, V_w, and hub height wind speed, V_H. Also, $v_{eq_{ws}}$ and $v_{eq_{ts}}$, are the equivalent wind speed, due to wind shear and tower shadow effects that are given as

$$v_{eq_{ws}} = V_H \left[\frac{\alpha(\alpha-1)}{8} \left(\frac{R}{H}\right)^2 + \frac{\alpha(\alpha-1)(\alpha-2)}{60} \left(\frac{R}{H}\right)^3 \cos 3\theta_b \right] \tag{5}$$

$$v_{eq_{ts}} = \frac{mV_H}{3R^2} \sum_{b=1}^{3} \left[\frac{a^2}{\sin^2\theta_b} \ln\left(\frac{R^2 \sin^2\theta_b}{x^2} + 1\right) - \frac{2a^2R^2}{R^2\sin^2\theta_b + x^2} \right] \tag{6}$$

where α, a, x, H and θ_b are the empirical wind shear exponent, tower radius, blade origin from tower midline, hub height and azimuthal angle of the blades, respectively.

2.2. Mechanical-Structural system

From the mechanical-structural interactions point of view, the blade edgewise motions are affected by the torsional oscillations. Moreover, the blades are coupled to the low speed shaft in the drive-train system and their dynamics can impact on the torsional modes. Hence, direct insights into the highly complex behavior of mechanical-structural dynamics result in a complete and accurate description for both edgewise and torsional dynamics.

2.2.1. Blade edgewise deflection modeling

For a horizontal axis three-bladed WT, Fig. 2 shows the schematic demonstration of the blade edgewise deflections, where the edgewise deflections are denoted by *z(r,t)* symbol which are as functions of the time and vary along the length of the blades [14].

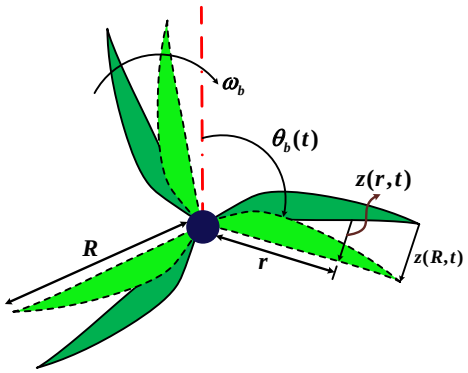

Fig. 2. Schematic demonstration of the blade-edgewise deflections

To obtain the dynamic model of the blade edgewise vibrations, the blades are generally assumed as flexible cantilever beams [15]. In practice, the first edgewise mode plays the principal role in edgewise resonant loads [13, 15]. Hence, in mathematical analyses, only the first edgewise mode is generally taken into account, in which, each beam is assumed to swing in the first mode frequency. Considering the kinetic and potential energies of the blades, ignoring the interaction between the blades and tower and neglecting the gravity effect, the motion equation of the blades in the edgewise direction, is given by [13]

$$Mz^{\cdot\cdot}(t) + Dz^{\cdot}(t) + Kz(t) = F_{\tan}(t) \tag{7}$$

where, M, D and K are the matrices corresponding to the mass, damping and stiffness, respectively, associated with the structural properties of the blades. Also, $z(t)$ is edgewise deflection matrix, $F_{tan}(t)$ is the matrix of the acting tangential forces on the blades. According to the (7) and parameters of the study system given in the Appendix, the natural frequency of the blade edgewise vibrations is equal to $2\pi\times1.95$ rad/sec.

Considering the collective pitch angle system as well as the isotropic rotor, all three blades will have the symmetrical edgewise motions. The tangential force is mainly affected from the wind loading conditions, and thus the effects of other factors can be ignored [13]. The aerodynamic aspects of the blade airfoil sections including the geometrical properties, wind speed inflow and the rotational speed of the blades are described as the blade element momentum (BEM) theory [11]. Using this theory and considering Fig. 3 and ignoring the aerodynamic interaction between different airfoil sections, the tangential force on each airfoil section at radial distance r from the hub can be expressed as

$$f_T(r,t) = f_L(r,t)\sin(\phi) - f_D(r,t)\cos(\phi) \tag{8}$$

where, f_L, f_D and Φ are the lift force, drag force and inflow angle, respectively. Assuming the homogenous wind turbulence over the rotor field, these variables can be written as follows

$$f_L(r,t) = \frac{1}{2}\rho V_{res}^{\ 2}(r,t)c(r)d(r)C_L(\gamma) \tag{9}$$

$$f_D(r,t) = \frac{1}{2}\rho V_{res}{}^2(r,t)c(r)d(r)C_D(\gamma) \tag{10}$$

$$\phi(r,t) = \tan^{-1}\left(\frac{(1-i_a)V_w}{r\omega_b(1+i_t)}\right) \tag{11}$$

$$\gamma(r,t) = \phi(r,t) - \theta_{sh-bh} - \beta \tag{12}$$

where $C_L(\gamma)$ and $C_D(\gamma)$ are the lift and drag coefficients of the blade elements, respectively. Further, $\theta_{sh\text{-}bh}$, $c(r)$, $d(r)$, i_a, i_t and β are the twist angle between the blades and hub, chord length, chord width, axial induction factor, tangential induction factor and pitch angle, respectively. V_{res} denotes the resultant wind velocity which can be written as

$$V_{res}(r,t) = \sqrt{(V_w(1-i_a))^2 + (\omega_b r(1+i_t))^2} \tag{13}$$

The linearized form of the tangential force around the operating points of the blade speed, ω_{b0}, operating wind speed, V_{w0}, operating pitch angle, β_0, and twist angle between the blade and hub, $\theta_{sh\text{-}bh0}$, is obtained as

$$\begin{aligned}\Delta f_{\tan} = &\Bigg[\left(f_{L_0}\cos\phi_0 + f_{D_0}\sin\phi_0 + \frac{1}{2}\rho A V_{res_0}^2 \left(\sin\phi_0 \frac{\partial C_L}{\partial\gamma} - \cos\phi_0 \frac{\partial C_D}{\partial\gamma}\right)\right)\frac{\partial\phi}{\partial\omega_b} + \\ &\left(\frac{1}{2}\rho A 2 V_{res_0}\left(C_{L_0}\sin\phi_0 - C_{D_0}\cos\phi_0\right)\right)\frac{\partial V_{res}}{\partial\omega_b}\Bigg]\Delta\omega_b + \\ &\left[\left(\frac{1}{2}\rho A V_{res_0}^2\left(\cos\phi_0\frac{\partial C_D}{\partial\gamma} - \sin\phi_0\frac{\partial C_L}{\partial\gamma}\right)\right](\Delta\beta + \Delta\theta_{sh-bh}) + \right. \\ &\Bigg[\left(f_{L_0}\cos\phi_0 + f_{D_0}\sin\phi_0 + \frac{1}{2}\rho A V_{res_0}^2 \left(\sin\phi_0 \frac{\partial C_L}{\partial\gamma} - \cos\phi_0 \frac{\partial C_D}{\partial\gamma}\right)\right)\frac{\partial\phi}{\partial V_w} + \\ &\left.\frac{1}{2}\rho A 2 V_{res_0}\left(C_{L_0}\sin\phi_0 - C_{D_0}\cos\phi_0\right)\right)\frac{\partial V_{res}}{\partial V_w}\Bigg]\Delta V_w\end{aligned} \tag{14}$$

where f_{L_0}, f_{D_0}, ϕ_0, V_{res_0}, C_{L_0} and C_{D_0} are the lift force, drag force, inflow angle, resultant speed, lift coefficient and drag coefficient at the operating point, respectively.

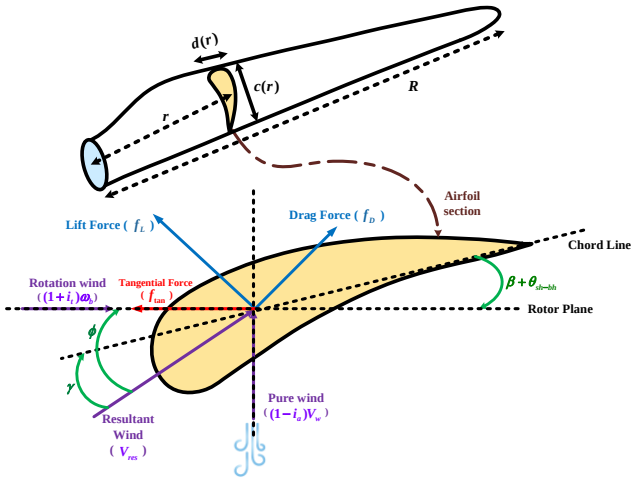

Fig. 3. Representation of aerodynamic velocities, flow angles and forces on a typical airfoil section

2.2.2. Drive-train modelling

The drive-train system is known as the transmitting stage between the aerodynamic system and power grid. This system commonly consists of the blades, hub, low speed shaft (LSS), gearbox, high speed shaft (HSS) and generator. According to the section 2.2.1, the edgewise deflections depend on the twist angle between the blade and hub ($\theta_{sh\text{-}bh}$) and the blade speed (ω_b) related to drive-train system. On the other hand, the blades can influence on the drive-train flexibilities. Thus, in this study, the interactions of the drive-train system with the blades are taken into account. Three mass drive-train model can realize this aim whose representation referred to the HSS is shown in Fig.4. In this model, the drive-train is split into three separate inertias coupled together through intermediate shafts having stiffness without inertia.

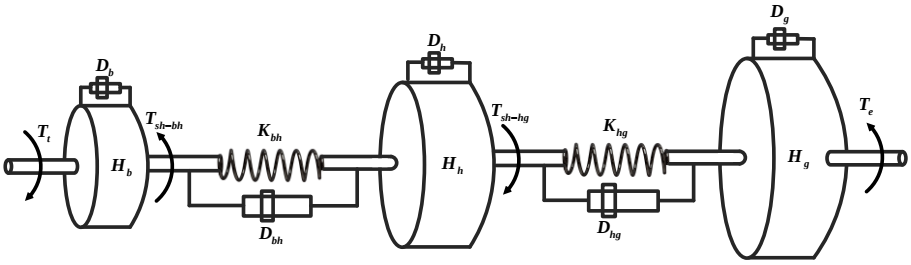

Fig. 4. Three mass drive-train model

The linearized form of the dynamic equations for the three mass drive-train model are given as follows:

$$\Delta T_t - \Delta T_{sh-bh} - D_b \Delta\omega_b = 2H_b \frac{d\Delta\omega_b}{dt} \tag{15}$$

$$\Delta T_{sh-bh} - \Delta T_{sh-hg} - D_h \Delta\omega_h = 2H_h \frac{d\Delta\omega_h}{dt} \tag{16}$$

$$\Delta T_{sh-hg} + \Delta T_e - D_g \Delta\omega_g = 2H_g \frac{d\Delta\omega_g}{dt} \tag{17}$$

$$\Delta T_{sh-bh} = k_{bh}\Delta\theta_{sh-bh} + D_{bh}(\Delta\omega_b - \Delta\omega_h) \tag{18}$$

$$\Delta T_{sh-hg} = k_{hg}\Delta\theta_{sh-hg} + D_{hg}(\Delta\omega_h - \Delta\omega_g) \tag{19}$$

$$\frac{d\Delta\theta_{sh-bh}}{dt} = \omega_B(\Delta\omega_b - \Delta\omega_h) \tag{20}$$

$$\frac{d\Delta\theta_{sh-hg}}{dt} = \omega_B(\Delta\omega_h - \Delta\omega_g) \tag{21}$$

where Δ is the symbol of the small variation around the operating point, ω_h and ω_g denote the angular speeds of the hub and generator, in (p.u.), respectively, $\theta_{sh\text{-}bh}$ and $\theta_{sh\text{-}hg}$ denote the shaft twist angles between the blade and the hub and also between the hub and the generator, in (p.u.), respectively, T_t and T_e refer to the torques associated to the turbine and generator, in (p.u.), respectively, and $T_{sh\text{-}bh}$ and $T_{sh\text{-}hg}$ refer to the torsional torques corresponding to the blade-hub and hub-generator shafts, in (p.u.), respectively, H_b, H_h and H_g are the inertia constants related to the blades, hub and generator, in (sec), respectively, k_{bh} and k_{hg} are the shaft stiffness coefficients associated to the blade-hub and hub-generator shafts, in (p.u./elec. rad), respectively, D_{bh} and D_{hg} are the mutual damping coefficients between the blade and hub and between the hub and generator in (p.u.), respectively, D_b, D_h and D_g are the self-damping coefficients corresponding to the blades, hub and generator in (p.u.), respectively, ω_B is defined as the base angular electrical frequency in (rad/sec).

The linearized form of the turbine torque around the operating point of the blade speed, ω_{b0}, wind speed, V_{w0}, and pitch angle, β_0, can be written as

$$\Delta T_t = \left(\frac{T_{t_0}}{V_{w_0}}\left(3 - \frac{\lambda_0}{C_{p_0}}\frac{\partial C_p}{\partial\lambda}\right)\right)\Delta V_w + \left(\frac{T_{t_0}}{C_{p_0}}\frac{\partial C_p}{\partial\beta}\right)\Delta\beta + \left(\frac{R\omega_{tB}}{V_{w_0}C_{p_0}}T_{t_0}\frac{\partial C_p}{\partial\lambda} - \frac{T_{t_0}}{\omega_{b_0}}\right)\Delta\omega_b \tag{22}$$

where T_{t_0}, V_{w_0}, λ_0 and C_{p_0} are the turbine torque, wind speed, blade tip speed ratio and power coefficient at the operating point, respectively, and ω_{tB} is the base angular frequency of the rotor. According to (15-21), the natural frequency of the drive-train system can be obtained as:

$$f_{1,2} = \frac{1}{2\pi}\left[\frac{-b}{2} \pm \frac{\sqrt{b^2 - 4c}}{2}\right]^{\frac{1}{2}} \tag{23}$$

where b and c in (23) are given by

$$b = -\left[k_{bh}\omega_B \left(\frac{1}{2H_b} + \frac{1}{2H_h}\right) + k_{hg}\omega_B \left(\frac{1}{2H_g} + \frac{1}{2H_h}\right) \right] \tag{24}$$

$$c = k_{bh}k_{hg}\frac{\omega_B}{4}(H_b + H_h + H_g)$$

For the study WT system with the parameters of Appendix, the natural frequencies of the drive-train system are equal to 2π×2.29 rad/sec and 2π×13.34 rad/sec. It is observed that the first drive-train natural frequency, i.e. 2π×2.29 rad/sec, is very close to the blade-edgewise resonance frequency, which is equal to 2π×1.95 rad/sec, for the study system.

2.3. PMSG modelling

The dynamic description of the PMSG in the d-q reference frame rotating at generator speed are given in (25)-(26) [26]. In these equations, all parameters and variables are expressed in per unit. The positive direction for the stator current is assumed into the generator, in addition the rotor type of the study PMSG is considered as non-salient pole.

$$v_{sdq} = R_s i_{sdq} + j\omega_g \psi_{sdq} + \frac{1}{\omega_B}\frac{d\psi_{sdq}}{dt} \tag{25}$$

$$\psi_{sdq} = L_s i_{sqd} + \psi_{pm} \tag{26}$$

where ψ, v and i are the flux, voltage, and current, and subscript s corresponds to the stator quantities. L_s and R_s are the inductance and resistance of the stator, ψ_{pm} is the amplitude of the stator flux linkage due to the rotor permanent magnet, and ω_g is the electrical angular speed of the generator which at steady state conditions is equal to the stator angular frequency, ω_s. Under steady state conditions and by neglecting the stator losses, the stator output active power and electromagnetic torque are obtained as [26]:

$$P_s = -\psi_{pm}\omega_g i_{sq} \tag{27}$$

$$T_e = \psi_{pm} i_{sq} \tag{28}$$

2.4. Control system of the PMSG-based WT

The operation regions of the variable speed WT is mainly composed of two regions: the MPPT region and rated power region, as shown in Fig. 5. In MPPT region the WT output power is adjusted by using power converters to realize maximum wind energy capture from the point A to point B. Once the wind speed exceeds its upper limit at Point B, the pitch control system starts to

work to prevent the mechanical stresses on the wind turbine structure which this region is called rated power region [27].

In this paper, the PMSG-WT is controlled in the power control mode and thus in sections 2.4.1 and 2.4.2, the control structures of the MSC and GSC are given to realize the power control mode operation.

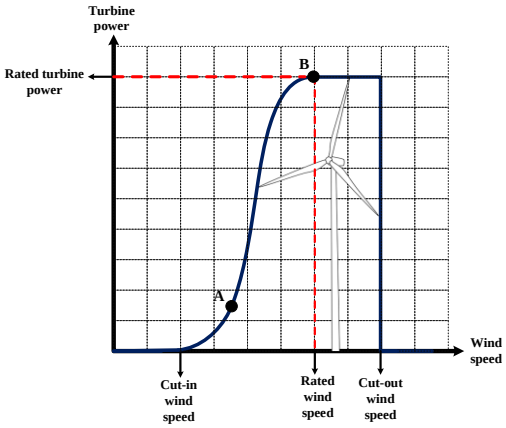

Fig. 5. Typical absorbed mechanical power versus wind speed in the variable speed WT

2.4.1. Control structure of the MSC

The main task of the MSC is regulation of the DC-link voltage to its reference value. This control scheme provides an appropriate LVRT capability under severe 3-phase voltage dips [26, 28]. Figure 6 shows the overall control structure of the MSC, including the stator inner current control loops and outer dc-link voltage control loop. In this structure, the reference value of the q-axis stator current, $i_{sq,ref}$, is obtained from the outer dc-link voltage controller. To optimize the generator current and minimize the ohmic losses, the stator d-axis reference current, $i_{sd,ref}$, is set to zero [29].

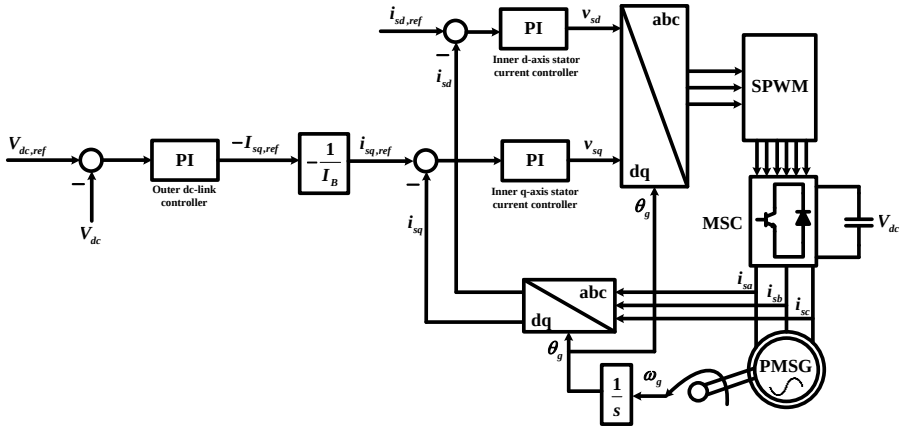

Fig. 6. Overall control structure of the MSC

2.4.2. Control structure of the GSC

The GSC is used to regulate the injected WT active power to the grid. In Fig. 7, the overall control structure of the GSC is shown, where v_{cd}, v_{cq}, i_{gd} and i_{cq} are dq-axes components of the GSC voltage and current in the grid voltage reference frame, in which the phase and frequency of the grid voltage are detected by the phase locked loop (PLL). The reference value of the active power, $P_{g,ref}$, is obtained through a predefined power-speed curve associated with aerodynamic characteristics of the WT blades. The GSC d-axis reference current, $i_{gd,ref}$, is generated by the active power controller, and also to operate the GSC in unity power factor, the GSC q-axis reference current, $i_{gq,ref}$, is set to zero [30].

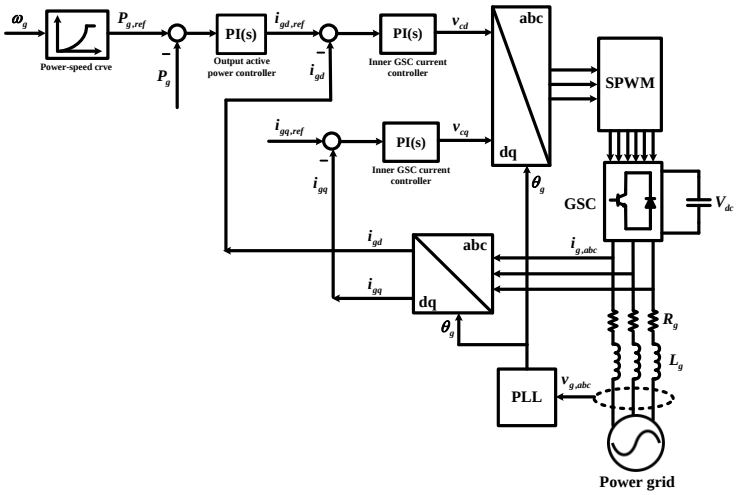

Fig. 7. Overall control structure of the GSC

2.4.3. Pitch control system

Figure 8 illustrates the closed-loop control of the pitch angle system, where $\omega_{g,ref}$, β_{ref}, β and τ_β are the maximum operating speed of the generator, pitch angle setpoint, actual pitch angle and time constant of the pitch actuator, respectively. In terms of the WT stability considerations and challenge of the aerodynamic model uncertainties, the parameters of the pitch angle controller are selected based on [31].

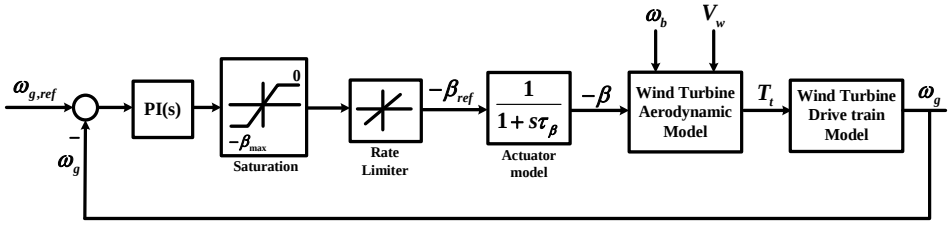

Fig. 8. Closed-loop control of the pitch angle system

3. Small signal and modal analysis of the WT

The complete dynamic model of the original closed loop PMSG-based WT comprising the dynamics of the electrical, mechanical-structural and control systems in linearized state-space form can be written as

$$\Delta \dot{x} = A.\Delta x + B.\Delta u \tag{29}$$

where A is an 20×20 state matrix, x is the vector of state variables, x=[i_{sd}, $x_{i_{sd}}, i_{sq}, x_{i_{sq}}, i_{gd}, x_{i_{gd}}, i_{gq}, x_{i_{gq}}, x_{P_g}, V_{dc}, x_{V_{dc}}, \beta, x_\beta, \omega_g, \omega_b, \omega_h, \theta_{sh-bh}, \theta_{sh-hg}, z, \dot{z}$]$^{\mathrm{T}}$, in which $x_{i_{sd}}, x_{i_{sq}}, x_{i_{gd}}, x_{i_{gq}}, x_{P_g}, x_{V_{dc}}$ and x_β are state variables corresponding to the integrator parts of the PI controllers of the MSC and GSC currents, output active power, dc-link voltage and pitch angle. Besides, u is the vector of exogenous inputs, u=[$V_w, \omega_{g,ref}, v_g, V_{dc,ref}$]$^{\mathrm{T}}$. Modal analysis is performed on an 8-pole, 5 MW, 690 V, 50 Hz PMSG-based WT system where the turbine characteristics is taken from the NREL 5MW wind turbine [32]. The rated parameters and key specifications of the turbine-generator are given in Appendix. Based on [13, 21, 33, 10], the fatigue loads at the rated operation area of the WT are more severe than the other areas. Hence, this section takes the operating points corresponding to the wind speed of 14 m/sec as a case study. Furthermore, the edgewise deflections on tip blade airfoils are more violent than the deflections on the other airfoils [14, 15]. Thus, all studies in this paper are performed based on the tip blade airfoil. Using (29), the eigenvalues of the state matrix are obtained, and then in order to exhibit the relationship between the modes and state variables, the participation factors of state variables are calculated. In Table 1, the system eigenvalues, corresponding frequencies, related damping ratios and respective dominant state variables are listed.

Table 1 Eigenvalues and dominant state variables for the WT in the power control mode

System Modes		Frequency (Hz)	Damping ratio	State variables with highest participation factor	
λ_1	-677.44	-	1	i_{sd}	
λ_2	-18.13	-	1	$x_{i_{sd}}$	
λ_3	–586.93	-	1	i_{sq}	
$\lambda_{4,5}$	$-628.32 \pm 0j$	-	1	i_{gd}	i_{gq}
$\lambda_{6,7}$	-45.92 ± 32.46j	5.17	0.82	V_{dc}	$x_{V_{dc}}$
λ_8	–18.18	-	1	$x_{i_{sq}}$	
λ_9	–62.83	-	1	x_{P_g}	
$\lambda_{10,11}$	$-6.28 \pm 0j$	-	1	$x_{i_{gd}}$	$x_{i_{gq}}$
$\lambda_{12,13}$	$-0.02 \pm 14.73j$	2.34	0.0014	θ_{sh-bh}	ω_g
$\lambda_{14,15}$	-3.12±83.87j	13.35	0.0372	θ_{sh-hg}	ω_h
$\lambda_{16,17}$	$-0.06 \pm 12.25j$	1.95	0.0049	z	$\dot{z}$
λ_{18}	–9.05	-	1	β	

$\lambda_{19,20}$	$-0.76 \pm 0.46j$	0. 73	0.86	x_β	ω_b

In Table 1, the modes $\lambda_{12,13}$, $\lambda_{14,15}$ and $\lambda_{16,17}$ are related to the mechanical-structural dynamics corresponding to the first and second resonant frequencies of the drive-train system as well as the single resonant frequency of the blade edgewise deflections, respectively. $\lambda_{12,13}$ are weakly damped modes associated with the shaft twist angle $\theta_{sh\text{-}bh}$ and generator speed ω_g with corresponding frequency and damping ratio of 2.34 Hz and 0.0014, respectively. Furthermore, $\lambda_{14,15}$ are the relatively weakly damped modes corresponding to the shaft twist angle $\theta_{sh\text{-}hg}$, and hub speed ω_h, with frequency and damping ratio of 13.35 Hz and 0.0372, respectively. The first torsional mode has the lower damping ratio compared to the second one, thus the modes $\lambda_{12,13}$ can be recognized as the dominant torsional modes. Moreover, the modes $\lambda_{16,17}$, are the weakly damped modes corresponding to the edgewise deflection, z, and the edgewise velocity, $\dot{z}$, with related frequency and damping ratio of 1.95 Hz and 0.0049, respectively.

The real modes λ_1, λ_2, λ_3, λ_8, λ_9 and λ_{18} are the fast damped modes corresponding to i_{sd}, $x_{i_{sd}}$, i_{sq}, $x_{i_{sq}}$, x_{P_g} and β, respectively, and $\lambda_{4,5}$, $\lambda_{6,7}$, $\lambda_{10,11}$ and $\lambda_{19,20}$ are the modes corresponding to the state variables i_{gd}, i_{gq}, V_{dc}, $x_{V_{dc}}$, $x_{i_{gd}}$, $x_{i_{gq}}$, x_β and ω_b. Since, these modes are well damped they are not dealt with in this study.

From Table 1, It can be observed that the mechanical-structural modes $\lambda_{12,13}$ and $\lambda_{16,17}$ have very low damping ratios, and also their natural frequencies are nearly similar. Besides, the tangential force, as the stimulating input to the edgewise vibrations, is directly affected by the shaft twist angle $\theta_{sh\text{-}bh}$ correlated to the modes $\lambda_{12,13}$. Hence, once the torsional modes are excited, the weakly damped oscillations appear on the tangential force which its harmonics may match with the edgewise eigenfrequency, $\lambda_{16,17}$, resulting in load amplification in the blades.

The blade passing phenomenon can be known as another source of the mechanical-structural resonances. Figure 9 shows the Campbell diagram of study WT, where the horizontal axis represents rotor speed and the vertical axis represents resonant frequencies. In Fig.9, the incline lines indicate the multiple blade passing harmonics (1P, 2P, etc.), while the shaded area specifies the operational speed range of the turbine. If there is an intersection between horizontal lines and any of the inclined lines, it may cause resonance problems of the WT. As shown in Figure 8, during the operational speed region of the WT, the eigenfrequencies of the edgewise and torsional encounter the fourth harmonic, 4P, of the blade passing effect. Because the 4P has small excitation energy, it seems unlikely that this harmonic causes the resonance occurrence in the structural-mechanical parts implying the fit design of the study WT. This issue will be assessed by nonlinear simulation results in the Section 6.

From Table 1 and Fig. 9, it can be concluded that to protect the blades and drive-train components, the control system should be planned such that the torsional and edgewise vibrations, caused by the aerodynamic and electric disturbances or by the blade passing turbulences are suppressed. For this aim, the proposed active mitigating control is described in the following section.

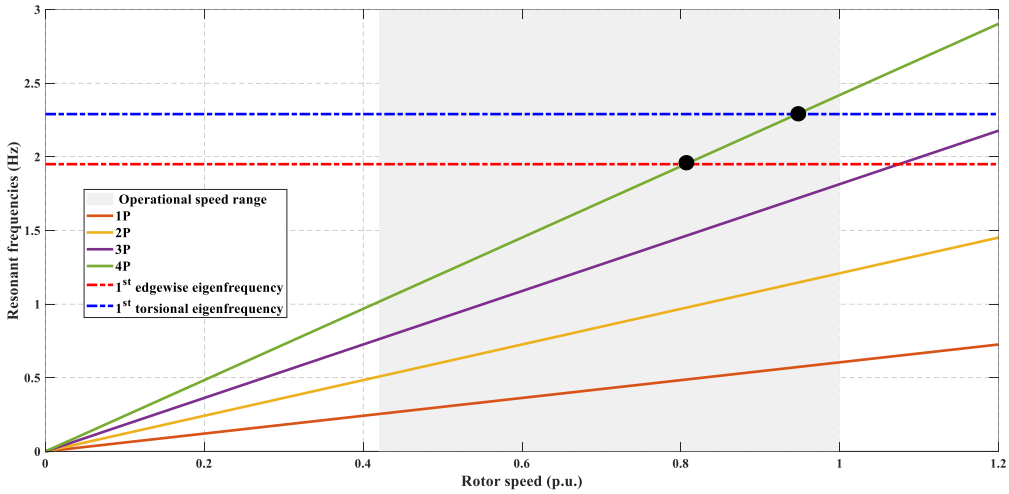

Fig. 9. Campbell diagram of the WT regarding the blade passing harmonics

4. Proposed active mitigating control

As mentioned in the previous section, the shaft twist angle $\theta_{sh\text{-}bh}$ has the highest participation factor in the torsional modes $\lambda_{12,13}$. Using (15)-(21), the dynamics of $\theta_{sh\text{-}bh}$ can be described as a function of (ω_b-ω_h), T_e, and ω_h, as given below:

$$\left(D_{bh}+\frac{2H_gD_{bh}}{k_{hg}\omega_B+D_{hg}s}\right)(\omega_b-\omega_h)+\left(k_{bh}+\frac{2H_gk_{bh}}{D_{hg}}(s-\frac{sk_{hg}\omega_B}{k_{hg}\omega_B+D_{hg}s})\right)\theta_{sh-bh}- \left(2(H_h+H_g)s+\frac{2H_hH_gs^3}{k_{hg}\omega_B+D_{hg}s}\right)\omega_h+Te=0 \quad (30)$$

Furthermore, considering (15-21), the dynamics of the $\theta_{sh\text{-}hg}$, with the highest participation in the modes $\lambda_{14,15}$, can also be described as a function of (ω_b-ω_h), T_e, and ω_h, as follows:

$$\left(D_{bh}+\frac{\omega_Bk_{bh}}{s}+\frac{2H_g\omega_Bk_{bh}}{D_{hg}}+\frac{2H_gD_{bh}s}{D_{hg}}\right)(\omega_b-\omega_h)-2H_gk_{hg}s\theta_{sh-hg}- \left(2H_hs+\frac{2H_gs}{D_{hg}}(2H_hs+D_{hg})\right)\omega_h+Te=0 \quad (31)$$

According to (30-31), suppressing the mechanical-structural loads, associated with the $\lambda_{12,13}$, $\lambda_{14,15}$ and $\lambda_{16,17}$ modes, can be realized if the electromagnetic torque contains a supplementary component as proportional to (ω_b-ω_h), as illustrated in Fig. 10, where α_{i_g} and K_E are the closed-loop band width of the GSC inner control loop and feedback gain, respectively. It can be observed from the Fig. 10 that the proposed active mitigating approach is realized by modifying the GSC output active power control loop. In this approach, the supplementary component proportional to (ω_b-ω_g) is added to $P_{g,ref}$.

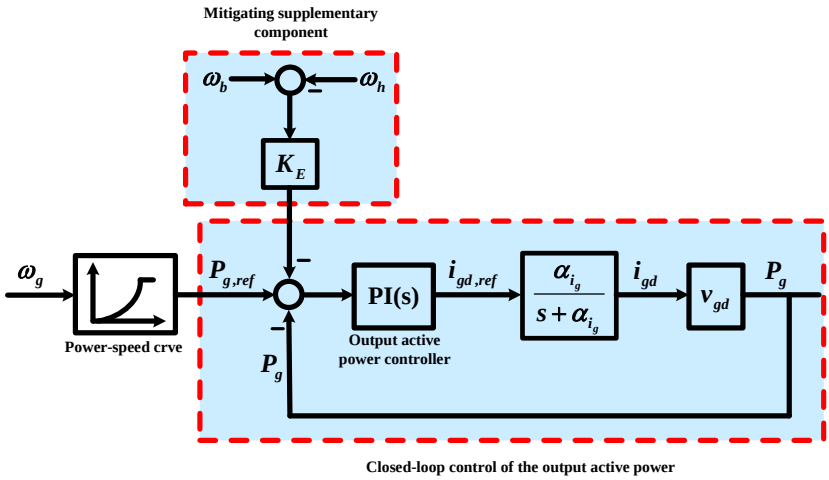

Fig. 10. Block diagram of the proposed active mitigating approach through the GSC control modification

Table 2 presents the modal analysis results related to the proposed active mitigating approach at the operating points corresponding to Vw=14m/sec, in which the feedback gain, K_E, is selected to 10. Comparing Tables 1 and 2, it is observed that by employing the proposed active mitigating control, the modes $\lambda_{12,13}$, are better damped compared to the original power loop control and the damping ratio is improved from 0.0014 to 0.42. Besides, the damping ratio of the modes $\lambda_{14,15}$ is relatively improved from 0.0372 to 0.063, whereas the damping ratios of the electrical modes remain relatively unchanged. Thus, the proposed active mitigating approach has not any adverse impact on electrical modes.

Table 2 Eigenvalues and dominant state variables for the WT with proposed active mitigating control

System Modes		Frequency (Hz)	Damping ratio	State variables with highest participation factor	
λ_1	-677.44	-	1	i_{sd}	
λ_2	-18.13	-	1	$x_{i_{sd}}$	
λ_3	–586.93	-	1	i_{sq}	
$\lambda_{4,5}$	$-628.32 \pm 0\,j$	-	1	i_{gd}	i_{gq}
$\lambda_{6,7}$	-30.76 ± 37.03j	5.89	0.64	V_{dc}	$x_{V_{dc}}$
λ_8	–18.17	-	1	$x_{i_{sq}}$	
λ_9	–75.52	-	1	x_{P_g}	
$\lambda_{10,11}$	$-6.3 \pm 0\,j$	-	1	$x_{i_{gd}}$	$x_{i_{gq}}$
$\lambda_{12,13}$	$-6.73 \pm 14.58\,j$	2.32	0.42	θ_{sh-bh}	ω_g
$\lambda_{14,15}$	-5.06+ ±80.58j	12.82	0.063	θ_{sh-hg}	ω_h
$\lambda_{16,17}$	$-0.06 \pm 12.25\,j$	1.95	0.0049	z	$\dot{z}$
λ_{18}	–9.39	-	1	β	
$\lambda_{19,20}$	$-0.76 \pm 0.46\,j$	0. 73	0.86	x_β	ω_b

Figures 11- 13 show the amplitudes of the frequency responses of the tangential force, blade-hub torsional torque and hub-generator torsional torque to the wind speed, V_w, and grid voltage, v_g, for

two control strategies in the cases with and without the proposed active mitigating approach. From the load mitigation point of view, the phase demonstration of the bode diagrams has no information, thus in Figs. 10-12 only the amplitudes of the frequency responses have been given. It is observed that during the resonances caused by the electrical or mechanical turbulences, the diagrams related to the proposed active mitigating control have smaller amplitudes in their frequency responses compared to the those without the active mitigating approach. According to Figs. 11-13, the proposed active mitigating control has no impact on the intrinsic edgewise damping. However, it prevents the edgewise resonant loads caused by the other oscillating loads with the similar eigenfrequency transmitted through the tangential force. This interaction can be observed by the simulation results for several case studies explained in Section 6.

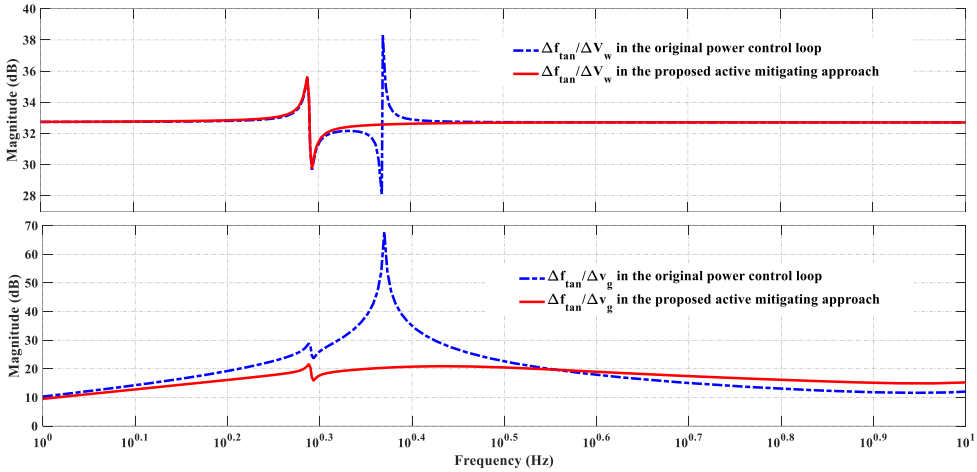

Fig. 11. The amplitude of the frequency responses of $\Delta f_{tan}/\Delta V_w$ and $\Delta f_{tan}/\Delta v_g$ for the cases with and without the proposed active mitigating approach

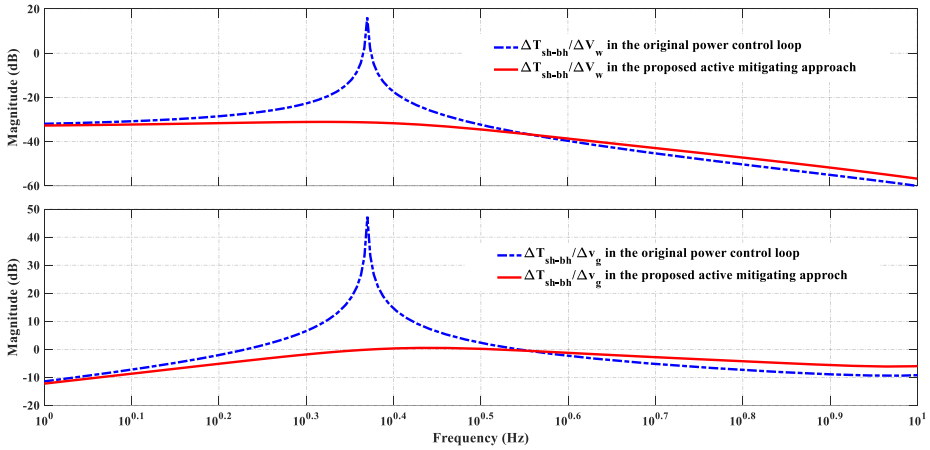

Fig. 12. The amplitude of the frequency responses of $\Delta T_{sh\text{-}bh}/\Delta V_w$ and $\Delta T_{sh\text{-}bh}/\Delta v_g$ for the cases with and without the proposed active mitigating approach

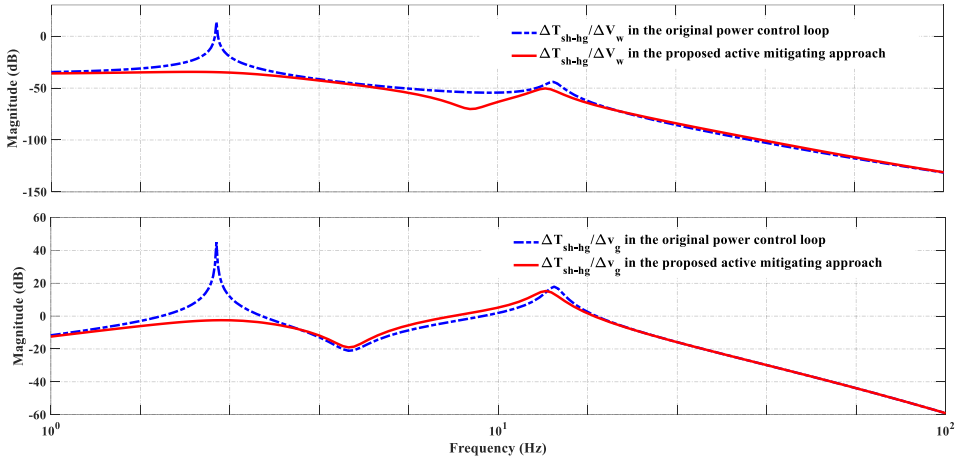

Fig. 13. The amplitude of the frequency responses of $\Delta T_{sh\text{-}hg}/\Delta V_w$ and $\Delta T_{sh\text{-}hg}/\Delta v_g$ for the cases with and without the proposed active mitigating approach

5. Sliding mode observer to estimate the required parameters of the proposed active mitigating approach

Implementing the proposed active mitigating approach depends on the instantaneous values of both the blade and hub speeds. Direct measuring the blade and hub speeds has difficulties, and thus they can be achieved by applying a sensorless approach. The SMO method can be expanded to realize the supplementary component in the GSC control system. This nonlinear observer has advantages as simple implementation, robust structure against uncertainties and fast response, nevertheless, it suffers from chattering phenomenon emerged in the observer output signals [34-36]. SMO based on the super twisting algorithm (STA) can effectively attenuate the chattering problem and provide precise estimation in the operational regions of the WT [34]. The starting point to design the SMO is achieved by forming the sliding mode surfaces in the state spaces. The designing procedure of the proposed SMO-based estimator is discussed in the following.

5.1. Designing the observer of the generator speed

To design the generator speed observer in the basis of the STA-SMO, first, the dynamic model of the PMSG transformed into the stationary reference frame is described in per unit as follows [37]

$$\frac{di_{s\alpha\beta}}{dt} = -\frac{\omega_B R_s}{L_s} i_{s\alpha\beta} + \frac{\omega_B}{L_s}(v_{s\alpha\beta} - E_{s\alpha\beta}) \tag{32}$$

where $i_{s\alpha\beta}$ and $v_{s\alpha\beta}$ are the α-β components of the stator voltages and currents, respectively, and also, $E_{s\alpha\beta}$ refer to the αβ components of the back electromotive force obtained as

$$\begin{cases} E_{s\alpha} = -\omega_g \psi_{pm} \sin\theta_r \\ E_{s\beta} = -\omega_g \psi_{pm} \cos\theta_r \end{cases} \tag{33}$$

where θ_r denotes the electrical rotor position angle. Equation (33) shows that the position and the speed of the generator can be extracted from the α-β back-EMFs. Using (32) the STA-SMO rule to estimate the α-β back-EMFs can be formulated as follows:

$$\frac{d\hat{i}_{s\alpha\beta}}{dt} = -\frac{\omega_B R_s}{L_s}\hat{i}_{s\alpha\beta} + \frac{\omega_B}{L_s}v_{s\alpha\beta} - \frac{\omega_B}{L_s}\left(k_1\int f(\sigma_{i_{s\alpha\beta}})d_t + k_2\sqrt{\left|\sigma_{i_{s\alpha\beta}}\right|}f(\sigma_{i_{s\alpha\beta}})\right) \tag{34}$$

where $\hat{i}_{s\alpha\beta}$ is the observed values of the α-β stator currents, $\sigma_{i_{s\alpha\beta}} = \hat{i}_{s\alpha\beta} - i_{s\alpha\beta}$, and k_1 and k_2 are the observer gains selected based on the stability analysis of the observer addressed in [34, 36]. Also, $f(\sigma_{i_{s\alpha\beta}})$ can be defined as the sign function or an approximation of it, for example a sigmoid function [36]. Provided the state variable of the observer converges to a band around the sliding mode surface, the estimated signals of the α-β back-EMFs are derived as

$$\hat{E}_{\alpha\beta} = \int k_1 f(\sigma_{i_{s\alpha\beta}})dt \tag{35}$$

The harmonic content present in the output signals of the back-EMF observer can be effectively smoothed by applying a Kalman filter in which the filtered signals are obtained as follows [34]:

$$\begin{cases}\bar{E}_\alpha = \int(\bar{E}_\beta\hat{\omega}_g - \tilde{E}_\alpha\eta)dt \\ \bar{E}_\beta = \int(\bar{E}_\alpha\hat{\omega}_g - \tilde{E}_\beta\eta)dt\end{cases} \tag{36}$$

where $\bar{E}_{\alpha\beta}$ are the filtered values of the observed α-β back-EMFs, η is the filter gain, $\tilde{E}_{\alpha\beta} = \bar{E}_{\alpha\beta} - \hat{E}_{\alpha\beta}$, and also $\hat{\omega}_g$ is the estimated generator speed discussed subsequently. Now, based on (33), the generator speed and rotor position can be estimated with $\bar{E}_{\alpha\beta}$ and the PLL structure shown in Fig. 14, where $\hat{\theta}_g$ is the estimated rotor position [34].

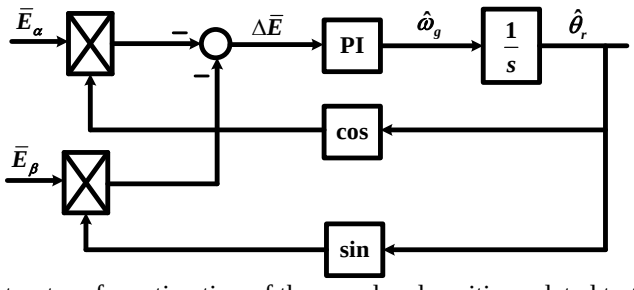

Fig. 14. PLL structure for estimation of the speed and position related to the generator

Considering Fig.13 and Eq. 33, and hypothesizing $\left|\theta_r - \hat{\theta}_r\right| < \frac{\pi}{6}$, we have $\Delta\bar{E} \approx \hat{\omega}_g\psi_{pm}(\theta_r - \hat{\theta}_r)$. Based on this result, the simplified closed-loop digram for the PLL structure is achived as Fig. 15.

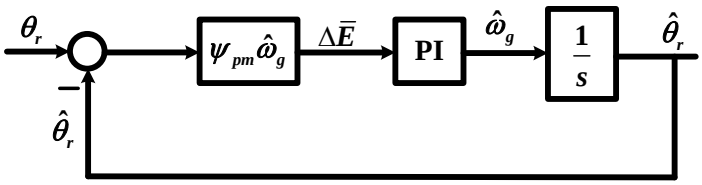

Fig. 15. The simplified closed-loop digram of the PLL structure for estimation of the speed and position related to the generator

5.2. Designing the observer of the hub-generator torsional torque

According to (17), the dynamic equation of the generator speed can be written as

$$\frac{d\omega_g}{dt} = \frac{\Delta T_{sh-hg}}{2H_g} + \frac{\Delta T_e}{2H_g} \tag{37}$$

Employing (37) and using the estimated generator speed obtained in the previous section, the STA-SMO rule for estimation of the hub-generator torsional torque can be obtained as

$$\frac{d\hat{\omega}_g}{dt} = \frac{1}{2H_g}\hat{T}_e + \frac{1}{2H_g}\left(k_3\int f(\sigma_{\omega_g})d_t + k_4\sqrt{|\sigma_{\omega_h}|}\,f(\sigma_{\omega_g})\right) \tag{38}$$

where $\hat{\omega}_g$ is the observed generator speed within the observer of the hub-generator torsional torque, and $\sigma_{\omega_g} = \hat{\omega}_g - \hat{\omega}_g$, k_3 and k_4 are the observer gains, $f(\sigma_{\omega_g})$ is considered as the sigmoid function, $\hat{T}_e$ is the estimated value of the electromagnetic torque acquired as $\hat{T}_e = \psi_{pm} i_{sq,ref}$. If the state variable of the observer reaches to the band of the sliding mode surface, the estimated signal of the hub-generator torsional torque is achieved as follows

$$\hat{T}_{sh-hg} = \int k_3 f(\sigma_{\omega_g})dt \tag{39}$$

5.3. Designing the hub speed estimator

From (19) and by using $\hat{\omega}_g$ and $\hat{T}_{sh-hg}$, estimated in Sections 5.1 and 5.2, the estimator of the hub speed is obtained as given in Fig. 16.

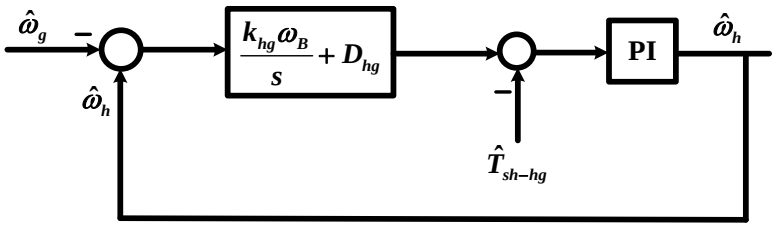

Fig. 16. Proposed structure for estimating the hub speed

5.4. Designing the blade-hub torsional torque observer

Considering (16), the mathematical law for the blade-hub torsional torque observer based on STA-SMO approach can be expressed as

$$\frac{d\bar{\omega}_h}{dt} = -\frac{1}{2H_h}\hat{T}_{sh-hg} + \frac{1}{2H_h}\left(\frac{k_5 f(\sigma_{\omega_h})}{s} + k_6\sqrt{|\sigma_{\omega_h}|}\, f(\sigma_{\omega_h})\right) \tag{40}$$

where $\bar{\omega}_h$ is the observed hub speed within the blade-hub torsional torque observer, $\sigma_{\omega_h} = \bar{\omega}_h - \hat{\omega}_h$, k_5 and k_6 are the observer gains, $f(\sigma_{\omega_h})$ is a sigmoid function, $\hat{T}_{sh-hg}$ and $\hat{\omega}_h$ are obtained by the former estimators introduced in Sections 5.2 and 5.3, respectively. If the hub speed, as the state variable of the observer, bounded to the sliding mode surface, the observed blade-hub torsional torque is obtained as

$$\hat{T}_{sh-bh} = \int k_5 f(\sigma_{\omega_h})dt \tag{41}$$

5.5. Designing the blade speed estimator

Similar to Section 5.3 and by using (18), the proposed structure for estimating the hub speed is obtained as shown in Fig. 17, where $\hat{\omega}_h$ and $\hat{T}_{sh-bh}$ com from the estimators introduced in Sections 5.3 and 5.4, respectively.

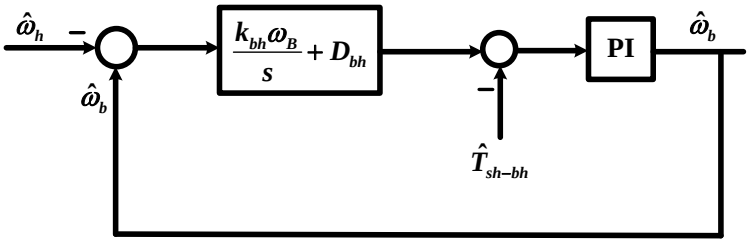

Fig. 17. Proposed structure for estimating the blade speed

6. Simulation Results

This section presents the simulation results to verify the effectiveness of the proposed active mitigating approach. The simulation platform is provided in MATLAB-Simulink environment wherein the detailed model of the WT, the proposed control approach and designed observer are established. The study system shown in Fig. 1 comprises a 5MW- 690V- 50Hz PMSG-based WT connected to a 20kV distribution grid through a 10km-20kV cable and step-up transformer. The simulation studies consists of three test cases presented in the following sections.

6.1. Test case1: Fatigue mitigating under wind speed variations

Figures 18-19 show the time domain simulations, frequency spectrums and rainflow cycles of the tangential force, tip blade edgewise deflections, blade-hub and hub-generator torsional torques, respectively, when a step change of wind speed occurs at t=20 s from 12 m/sec to 14 m/sec. Once the wind speed is changed, in the case without the proposed mitigating approach, transient vibrations are appeared on the WT structural-mechanical responses. By using the proposed active mitigating approach, the vibration amplitude of the tangential force, edgewise deflection, blade-hub torsional torque and hub-generator torsional torque decreases by 70%, 50%, 800% and 350%, respectively, compared to the case without the proposed approach. Besides, according to Figs. 18-19, the simulation results of the proposed active mitigating approach have the less rainflow cycles. Hence, the proposed active mitigating approach can considerably alleviate the fatigues related to the edgewise and torsional vibrations.

The other harmonics with the lower orders than the edgewise frequency arise from the blade passing phenomenon. Although BPPh oscillations have adverse effect on the waveforms with and without the proposed mitigating approach, but they not able to excite the mechanical-structural modes.

Figure 20 demonstrates time responses of the pitch angle, DC-link voltage and delivered active power to the grid against the step change of wind speed. It can be seen that the proposed active mitigating control not only does not impose additional burden on the pitch system and DC-link voltage, but also improves their responses.

Figure 21 depicts the estimated and actual values of the generator, hub and blade speeds, respectively, while the WT encounters to the mentioned wind speed change. Considering Fig. 20, the estimated and actual signals are very close to each other with very small error, less than 0.05%.

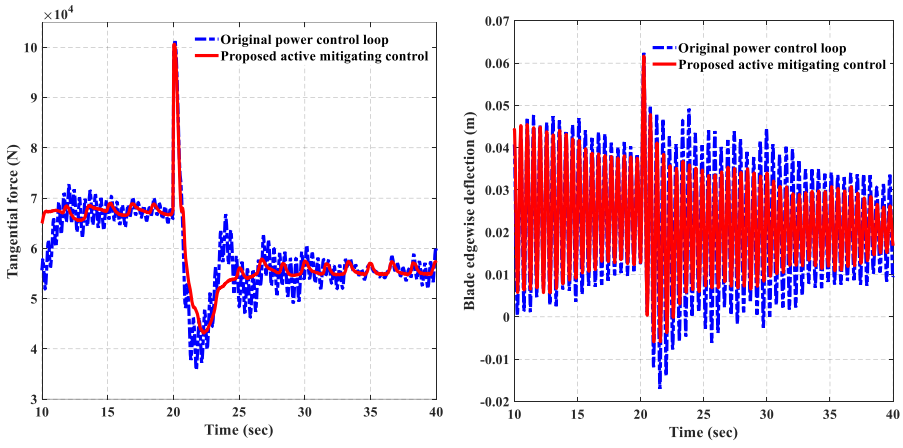

(a) (b)

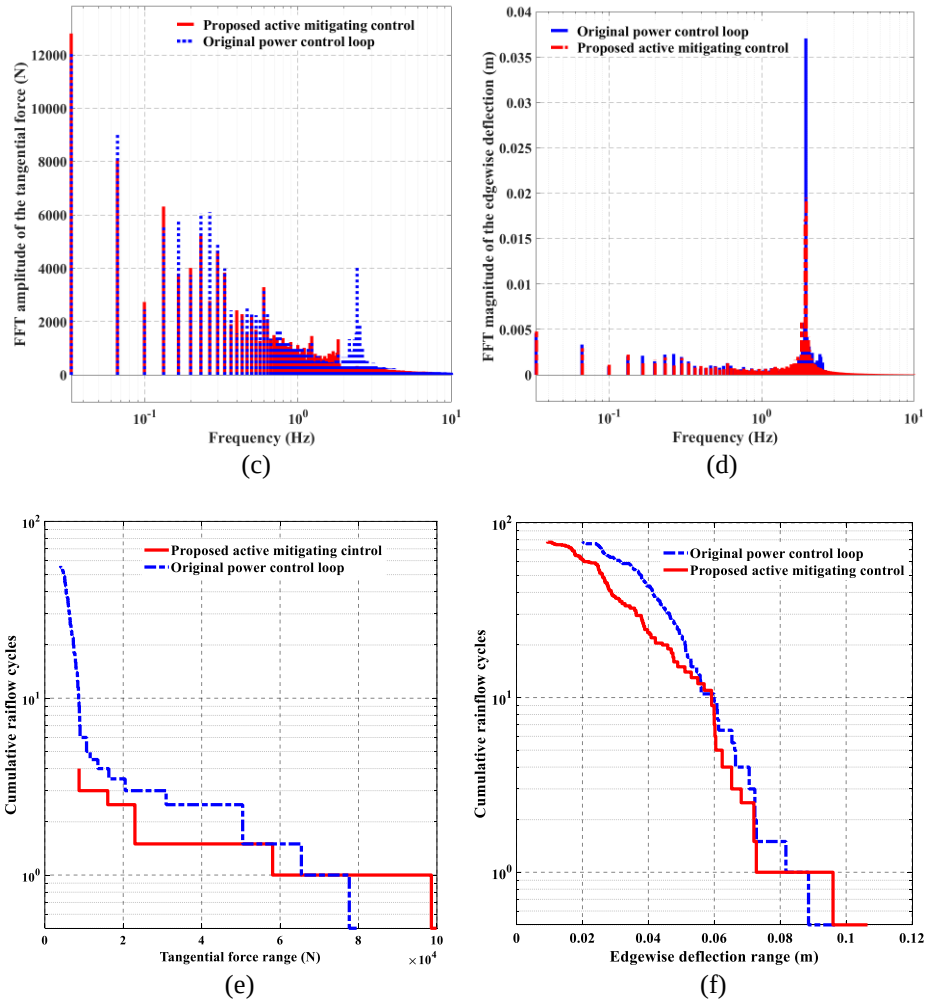

Fig. 18. Time domain simulations, frequency spectrums and rainflow cycles for the tangential force and edgewise deflection under the step change of the wind speed for two cases with and without the proposed active mitigating control

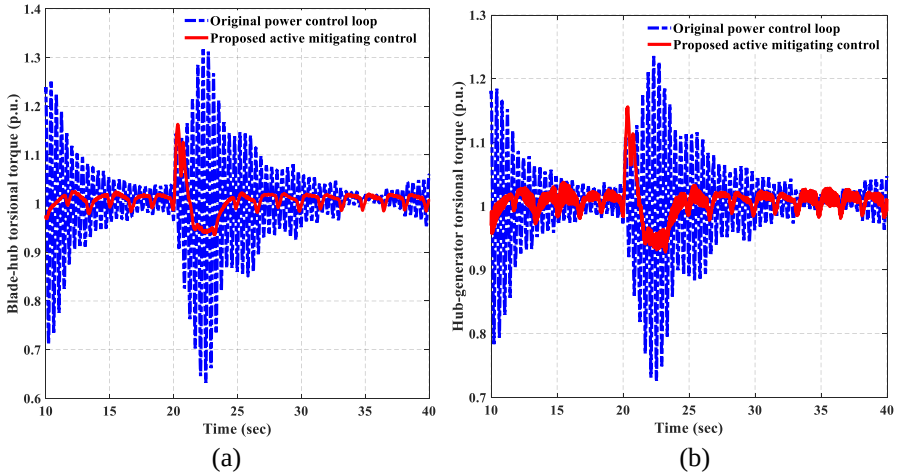

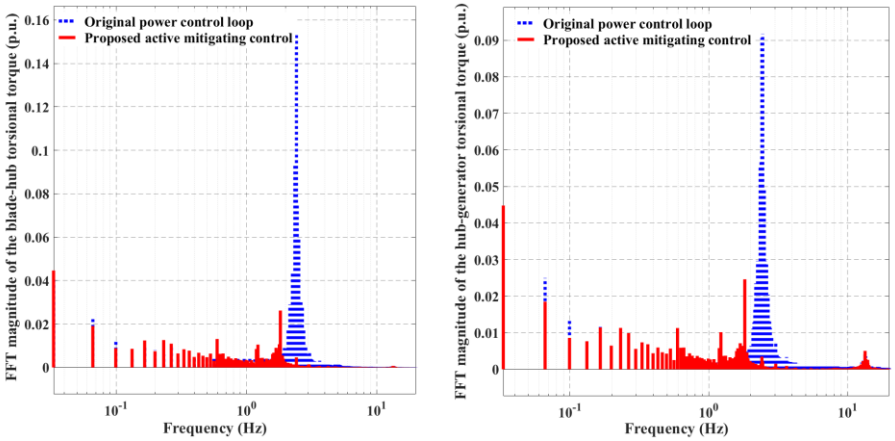

(c) (d)

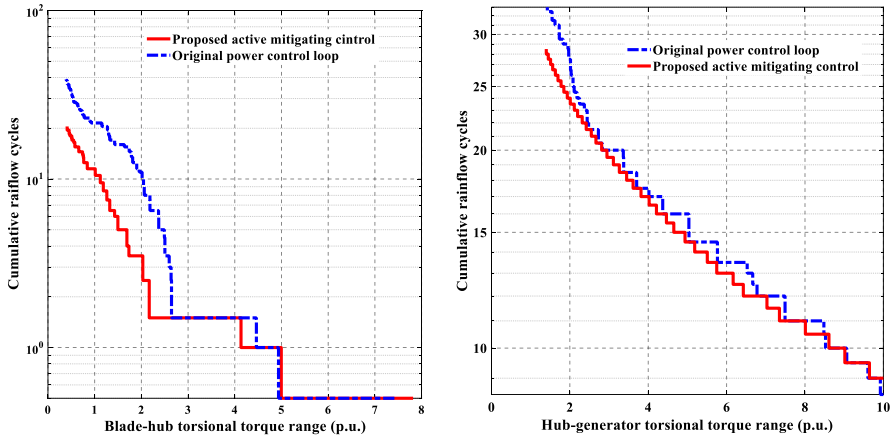

(e) (f)

Fig. 19. Time domain simulations, frequency spectrums and rainflow cycles of the blade-hub torsional torque and hub-generator torsional torque under step change of the wind speed for two caes with and without the proposed active mitigating control

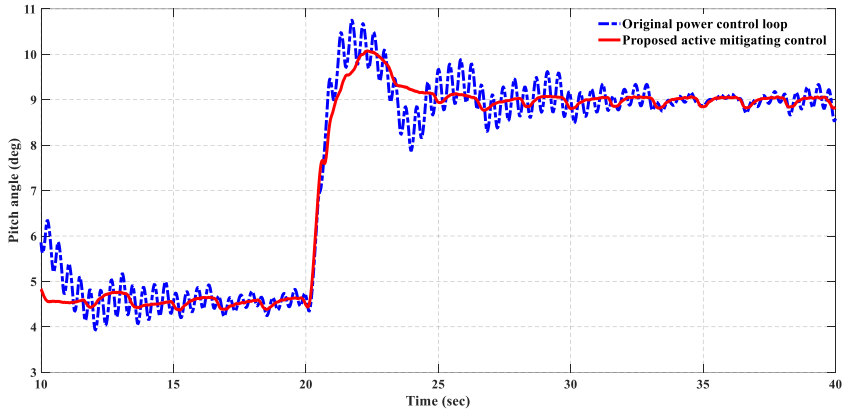

(a)

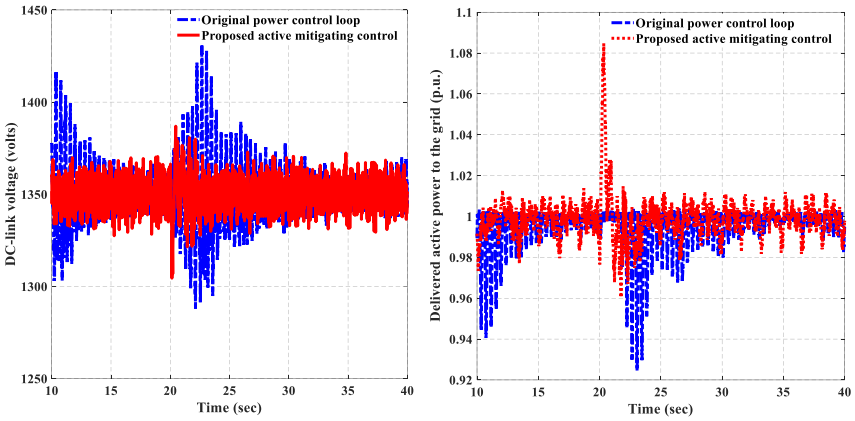

(b) (c)

Fig. 20. Time response of the pitch angle, DC-link voltage and output active power to the step change of the wind speed for two cases with and without the proposed active mitigating control

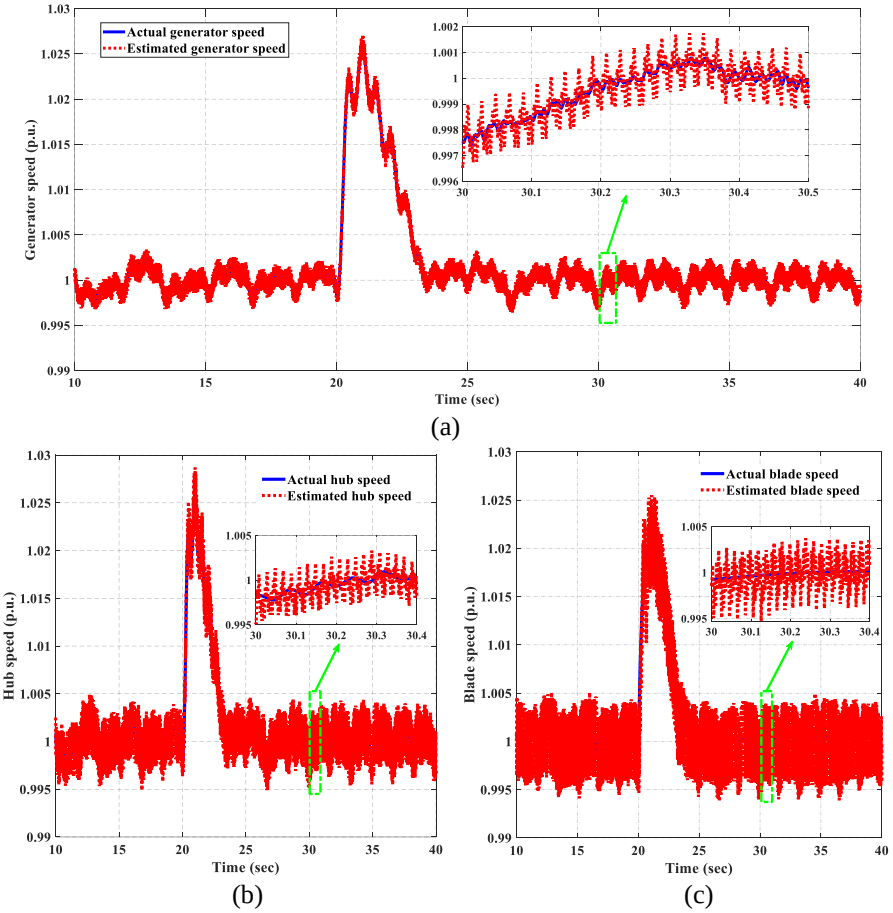

(a)

(b) (c)

Fig. 21. Time responses of the actual and estimated values of the generator, hub and blade speeds to the step change of the wind speed by applying the proposed active mitigation approach

6.2. Test case2: Fatigue mitigating under grid voltage dip

Figures 22-23 depict the time domain simulations, frequency spectrums and rainflow cycles of the tangential force, tip blade edgewise deflections, blade-hub and hub-generator torsional torques, respectively, when the grid is subjects to a 80% voltage dip with duration of 500 milliseconds at t=25s. It is evident that, by using the proposed active mitigating approach, large fluctuations corresponding to the structural-mechanical responses can be considerably alleviated. By using the proposed approach, vibration amplitudes of the tangential force, edgewise deflection, blade-hub torsional torque and hub-generator torsional torque decreases by 200%, 50%, 800% and 300%, respectively. The rainflow responses of Figs. 22-23 confirm the positive impact of the proposed approach. In addition, Fig. 24 shows that under the grid voltage dip the proposed control not only does not enter any burden on the pitch and electrical parts, but also effectively alleviates their transient responses.

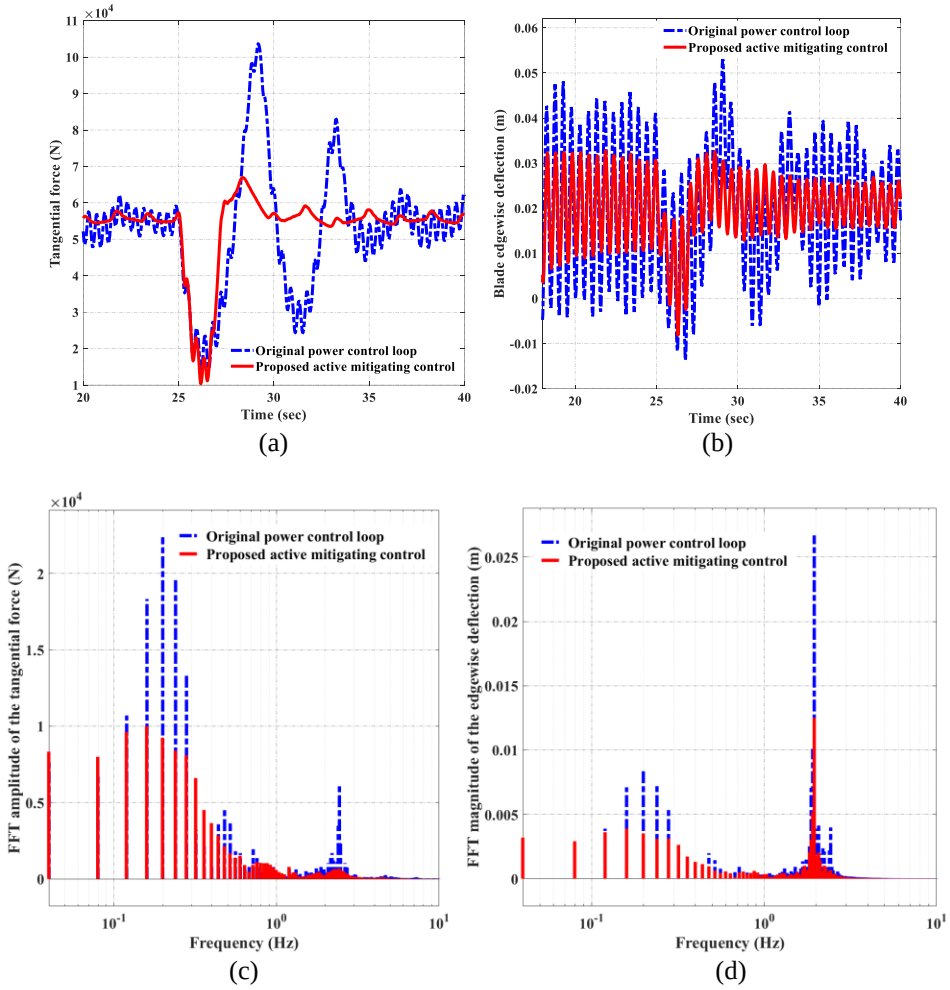

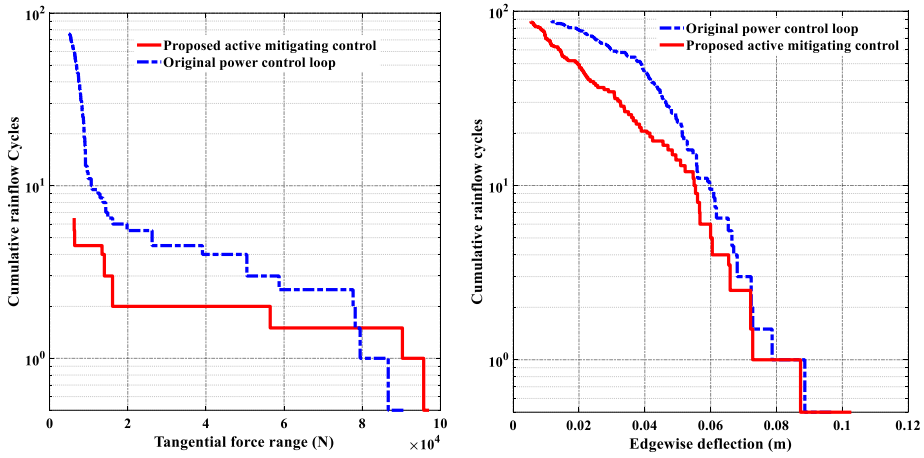

(e) (f)

Fig. 22. Time domain simulations, frequency spectrums and rainflow cycles for the tangential force and edgewise deflection against a grid voltage dip for two cases with and without the proposed active mitigating approach

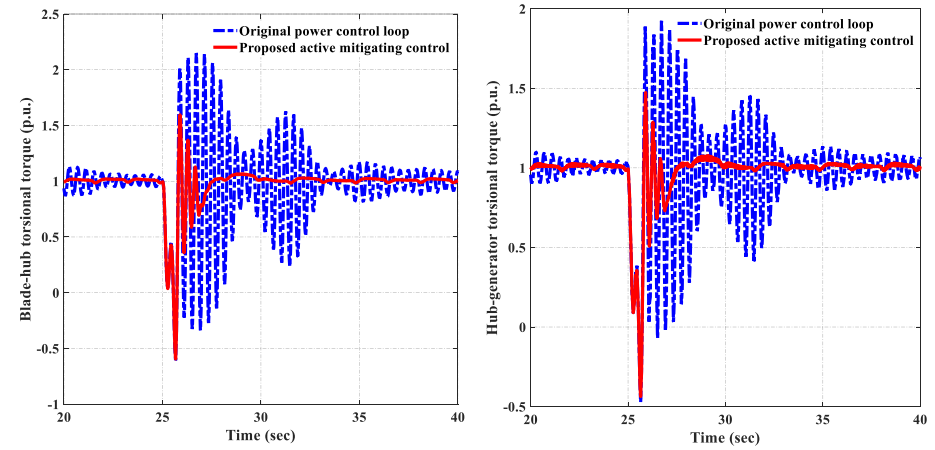

(a) (b)

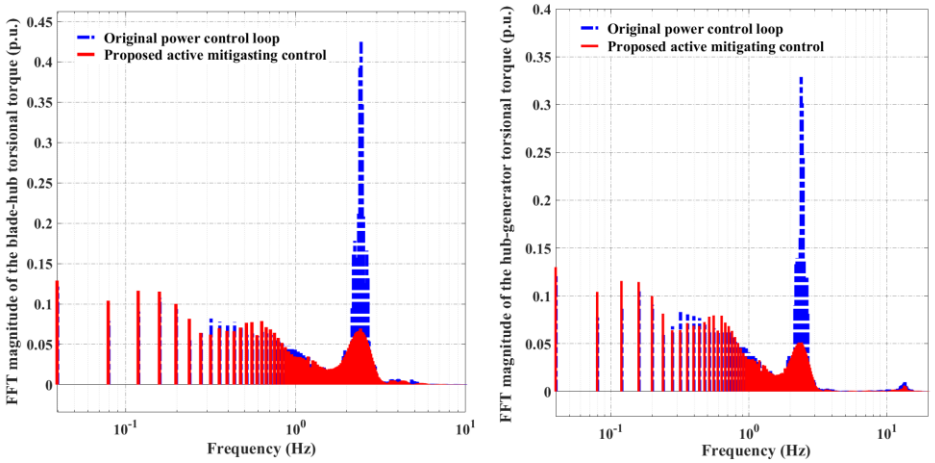

(c) (d)

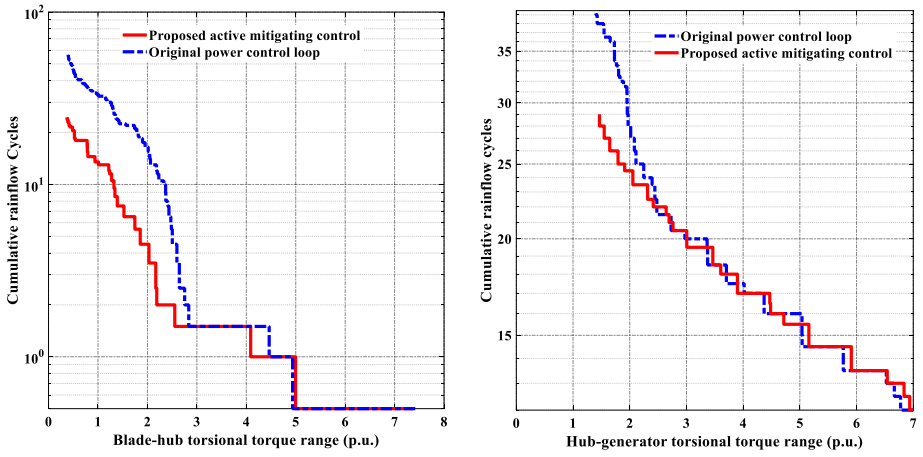

(e) (f)

Fig. 23. Time and frequency domain simulation and rainflow cycles of the blade-hub torsional torque and hub-generator torsional torque against a grid voltage dip for two cases with and without the proposed active mitigating approach

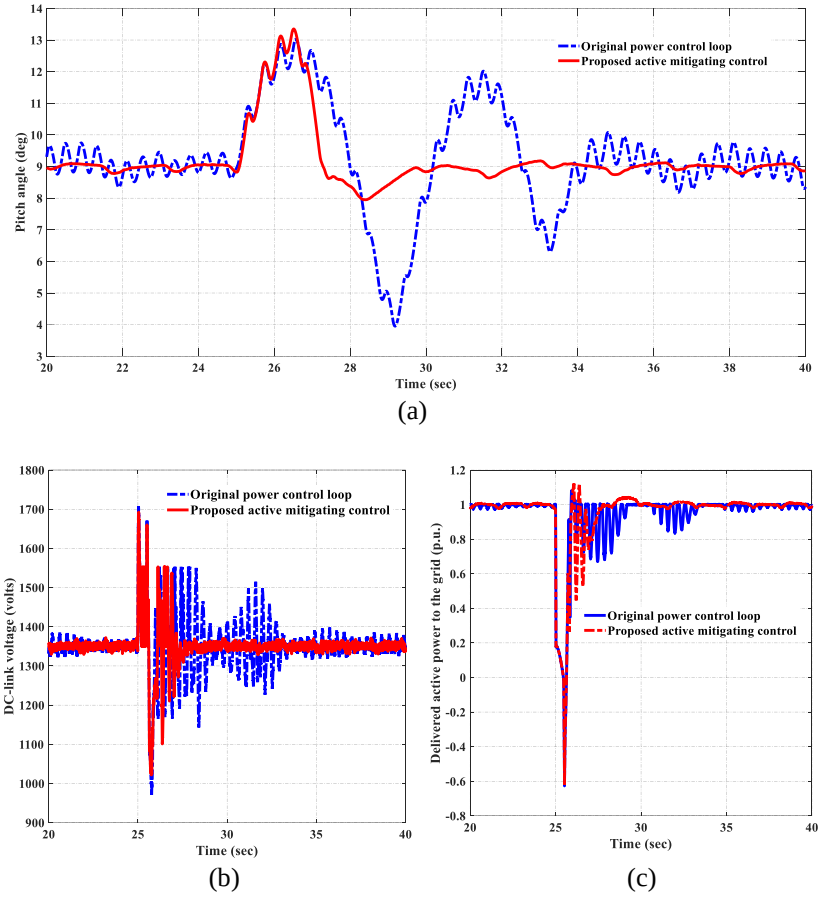

(a) (b) (c)

Fig. 24. Time response of the pitch angle, DC-link voltage and output active power to a grid voltage dip for two cases with and without the proposed active mitigating approach

6.3. Test case3: Performance evaluation of the proposed active mitigating approach under parametric uncertainties

Figure 25 examines the performance of the proposed active mitigating control under 50% overestimation in shaft stiffness coefficients, $k_{sh\text{-}bh}$ and $k_{sh\text{-}hg}$. It is observed that the performance of the proposed active mitigating approach is not affected by the mentioned uncertainty, and this approach can be recognized as a robust and reliable method in the control system of the PMSG-based WT.

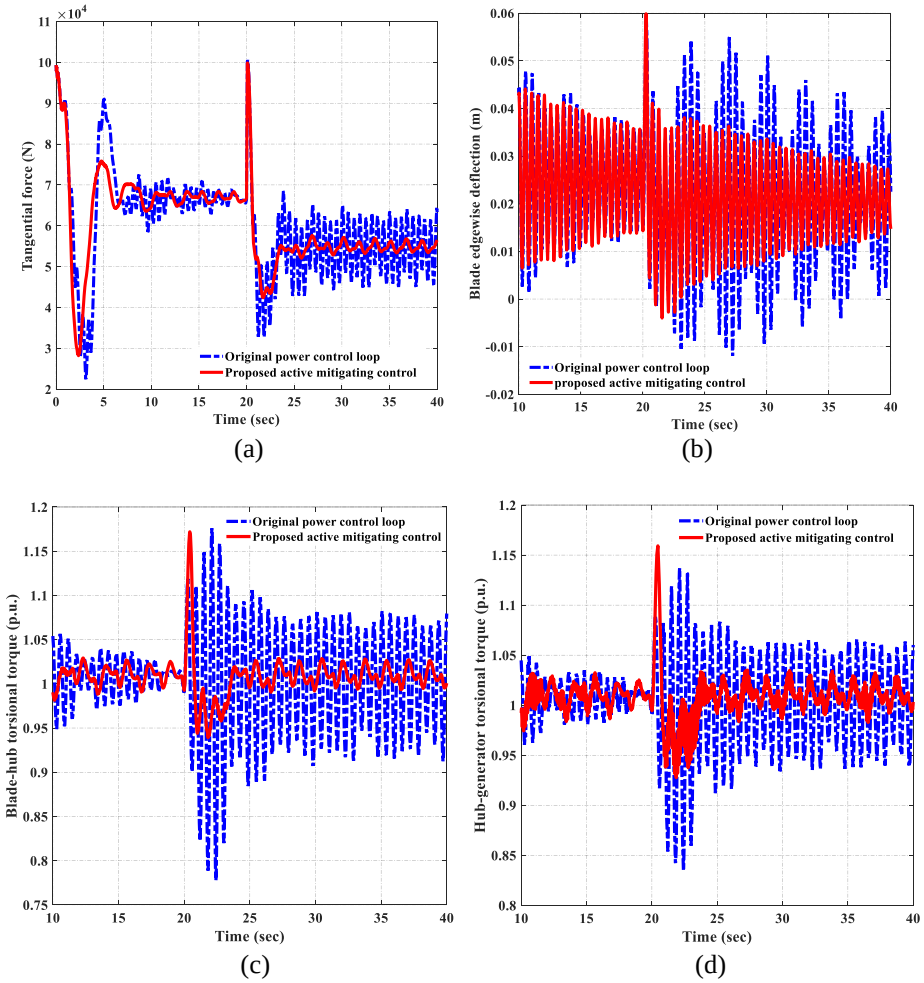

Fig. 25. Time responses of the tangential force, blade edgewise deflections, blade-hub torsional torque and hub-generator torsional torque to a step change of the wind speed, under 50% overestimation in the shaft stiffness coefficients

7. Conclusion

This paper proposes an active mitigating control for both torsional and edgewise vibrations in a large scale PMSG-based WT connected to the grid. The proposed control is established based on a high fidelity dynamic model for the mechanical-structural system. This model presents the impact of the blade flexibilities on the drive-train system, and provides the effect of the torsional

resonant loads on the blade edgewise deflections. In the proposed control, the GSC outer control loop is modified to make an auxiliary mitigating term in the control loop. This term is proportional to the difference between the blade and hub speeds. These speeds are estimated by a robust sensorless method in which the observer structure is designed based on the SMO technique. Small signal stability analysis and simulation results show that the proposed active mitigating control attenuates the torsional and edgewise vibrations once the WT is subjected to a turbulence. Further, the proposed control is robust against the parametric uncertainties.

References

[1] A. Awada, R. Younes, and A. Ilinca, "Review of Vibration Control Methods for Wind Turbines," *Energies*, vol. 14, no. 11, p. 3058, May. 2021.

[2] B. Fitzgerald, B. Basu, " Vibration control of wind turbines: Recent advances and emerging trends," *Int. J. Sustain. Mater. Struct. Syst*, vol. 4, pp. 347–372, Nov. 2020.

[3] H. Zuo, K. Bi and H. Hao, "A state-of-the-art review on the vibration mitigation of wind turbines", *Renewable Sustain. Energy Rev.*, vol. 121, Apr. 2020.

[4] R. M. D., E. Gonzalez and J. Malero, "Wind Turbine Failures-Tackling Current Problems in Failure Data Analysis", *Journal of Physics: Conference Series*, vol. 753, no. 7, 2016.

[5] Z. Li, S. Tian, Y. Zhang, H. Li, and M. Lu, "Active Control of Drive Chain Torsional Vibration for DFIG-Based Wind Turbine," *Energies*, vol. 12, no. 9, p. 1744, May. 2019.

[6] Y. Wang, Y. Guo, D. Zhang, H. Liu and O. Song, "Analysis and mitigation of the drive train fatigue load for wind turbine with inertial control, "*International Journal of Electrical Power & Energy Systems*, Vol. 136, p. 107698, March. 2022.

[7] M. Rahimi, A. Beiki, "Efficient modification of the control system in PMSG-based wind turbine for improvement of the wind turbine dynamic response and suppression of torsional oscillations," *Int. Trans. Electr. Energy Syst*, vol. 28, no. 8, p. 2578, Aug. 2018.

[8] A. Beiki, M. Rahimi, "An efficient sensorless approach for energy conversion enhancement and damping response improvement in permanent magnet synchronous generator (PMSG) based wind turbines," *Int. Trans. Electr. Energy* Syst, vol. 29, no. 1, p. 2684, Jul. 2019.

[9] E. Mohammadi, R. Fadaeinedjad and G. Moschopoulos, "Implementation of internal model based control and individual pitch control to reduce fatigue loads and tower vibrations in wind turbines", *J. Sound Vib.*, vol. 421, pp. 132-152, May. 2018.

[10] H. Liu, Q. Tang, Y. Chi, Z. Zhang, and X. Yuan, "Vibration reduction strategy for wind turbine based on individual pitch control and torque damping control", *Int. Trans. Electr. Energ. Syst.*, vol. 26, pp. 2230-2243, Oct. 2016.

[11] M. O. Hansen, Aerodynamics Wind Turbines, London, U.K:Earthscan, 2008.

[12] I. P. Girsang, J. S. Dhupia, E. Muljadi, M. Singh and J. Jonkman, "Modeling and Control to Mitigate Resonant Load in Variable-Speed Wind Turbine Drivetrain," in IEEE Journal of Emerging and Selected Topics in Power Electronics, vol. 1, no. 4, pp. 277-286, Dec. 2013.

[13] G. P. Prajapat, N. Senroy and I. N. Kar, "Wind Turbine Structural Modeling Consideration for Dynamic Studies of DFIG Based System," in IEEE Transactions on Sustainable Energy, vol. 8, no. 4, pp. 1463-1472, Oct. 2017.

[14] A. Staino and B. Basu, "Dynamics and control of vibrations in wind turbines with variable rotor speed", *J. Eng. Struct.*, vol. 56, pp. 58-67, Nov. 2013.

[15] A. Staino, B. Basu and S. R. K. Nielsen, "Actuator control of edgewise vibrations in wind turbine blades", J. Sound Vib., vol. 331, pp. 1233-1256, Mar. 2012.

[16] J. Licari, C. E. Ugalde-Loo, J. Liang, J. Ekanayake and N. Jenkins, "Torsional damping considering both shaft and blade flexibilities", *Wind Eng.*, vol. 36, pp. 181-196, 2012.

[17] J. Licari, C. Ugalde-Loo, J. Ekanayake and N. Jenkins, "Comparison of the performance and stability of two torsional vibration dampers for variable-speed wind turbines", *J. Wind Energy*, vol. 18, no. 10, pp. 1545-1559, Jun. 2015.

[18] L. Liu and D. Xie, "Performance comparison of two different filter design approaches for torsional vibration damping in a doubly fed induction generator-based wind turbine", *J. Eng.*, vol. 2015.

[19] L. Liu, D. Xie, H. Chu and C. Gu, "A damping method for torsional vibrations in a DFIG wind turbine system based on small-signal analysis", *Electric Power Compon. Syst.*, vol. 45, no. 5, pp. 560-573, Mar. 2017.

[20] A. Bensalah, G. Barakat, and Y. Amara, "Electrical Generators for Large Wind Turbine: Trends and Challenges," *Energies*, vol. 15, no. 18, p. 6700, Sep. 2022, doi: 10.3390/en15186700.

[21] M. Rahimi, "Improvement of energy conversion efficiency and damping of wind turbine response in grid connected DFIG based wind turbines", *Int. J. Elec. Power*, vol. 95, pp. 11-25, 2018.

[22] E. Van der Hooft, P. Schaak and T. Van Engelen, "Wind turbine control algorithms", 2003.

[23] S. Das, N. Karnik and S. Santoso, "Time-domain modelling of tower shadow and wind shear in wind turbines", *ISRN Renew. Energy*, vol. 2011, pp. 890582-1-890582-11, 2011.

[24] A. G. Abo-Khalil, S. Alyami, K. Sayed and A. Alhejji, "Dynamic modeling of wind turbines based on estimated wind speed under turbulent conditions", *Energies*, vol. 12, no. 10, pp. 1907, May 2019.

[25] D. S. L. Dolan and P. W. Lehn, "Simulation model of wind turbine 3p torque oscillations due to wind shear and tower shadow", *IEEE Transactions on Energy Conversion*, vol. 21, no. 3, pp. 717-724, Sept. 2006, doi: 10.1109/TEC.2006.874211.

[26] M. Rahimi, "Mathematical modeling dynamic response analysis and control of pmsg-based wind turbines operating with an alternative control structure in power control mode", *International Transactions on Electrical Energy Systems*, vol. 27, no. 12, pp. e2423, 2017.

[27] Y. Joo and J. Back, "Power regulation of variable speed wind turbines using pitch control based on disturbance observer", *J. Elect. Eng. Technol.*, vol. 7, pp. 273-280, 2012.

[28] Y. Abdollahi, M. Rahimi, A. Halvaei-Niasar, "Control and performance assessment of grid connected PMSG-based wind turbine equipped with diode bridge rectifier and boost converter using three different control strategies," *Scientia Iranica*, Jul. 2022.

[29] M. Chinchilla, S. Arnaltes and J. C. Burgos, "Control of permanent-magnet generators applied to variable-speed wind-energy systems connected to the grid," in IEEE Transactions on Energy Conversion, vol. 21, no. 1, pp. 130-135, Mar. 2006.

[30] A. Safaeinejad, M. Rahimi, "Control and performance analysis of grid-connected variable speed wind turbine with dual stator-winding induction generator for the contribution of both stator windings in active power transmission", *IET Renewable Power Generation*, vol. 14, pp. 2348-2358, Oct. 2020.

[31] M. Rahimi and M. Asadi, "Control and dynamic response analysis of full converter wind turbines with squirrel cage induction generators considering pitch control and drive train dynamics", *Int. J. Electr. Power Energy Syst.*, vol. 108, pp. 280-292, Jun. 2019.

[32] J. Jonkman, S. Butterfield, W. Musial and G. Scott, *Definition of a 5-mw reference wind turbine for offshore system development*, Feb. 2009.

[33] J. Licari, C. E. Ugalde-Loo, J. Liang, J. Ekanayake and N. Jenkins, "Torsional damping considering both shaft and blade flexibilities," *Wind Eng.*, vol. 36, pp. 181-196, 2012.

[34] L. Zhang, J. Bai, J. Wu, "Speed Sensor-Less Control System of Surface-Mounted Permanent Magnet Synchronous Motor Based on Adaptive Feedback Gain Supertwisting Sliding Mode Observer," *Journal of Sensors.*, vol. 2021, p. 8301359, sept. 2021.

[35] L. Guo, H. Wang, N. Jin, L. Dai, L. Cao and K. Luo, "A Speed Sensorless Control Method for Permanent Magnet Synchronous Motor Based on Super-Twisting Sliding Mode Observer," 2019 14th IEEE Conference on Industrial Electronics and Applications (ICIEA), 2019, pp. 1179-1184.

[36] B. Marcell, U. Gudrun, Sensorless Control of PMSM Drive Using Sliding-Mode-Observers, 2020.

[37] G. Koch, T. Gabbi, G. Henz, R. P. Vieira and H. Pinheiro, "Sensorless technique applied to PMSG of WECS using sliding mode observer," 2015 IEEE 13th Brazilian Power Electronics Conference and 1st Southern Power Electronics Conference (COBEP/SPEC), 2015, pp. 1-6.

Appendix A

Specifications of wind turbine model

Symbol	Quantity	Value
P_n	Rated output power	5 MW
R	Blade radius	63 m
n_g	Gearbox ratio	62
ρ	Air density	1.222 kg/m^3
J_b	Blade moment of inertia	2.84×10^7 kgm^2
J_h	Hub moment of inertia	753519 kgm^2
H	Hub height	90 m
$K_{sh\text{-}bh}$	Blade-hub shaft stiffness coefficient	6.6×10^8 N.m/rad
$K_{sh\text{-}hg}$	Hub-generator shaft stiffness coefficient	3.66×10^9 N.m/rad
a	Tower radius	2.4 m
α	Wind shear component	0.3
x	Blade origin from tower midline	5 m
τ_β	Time constant of the pitch actuator	0.1 sec
M	Overall mass of the blades	17740 Kg
K	Stiffness coefficient of the blades structure	2.67×10^6 N/m

Appendix B

Specifications of PMSG

Symbol	Quantity	Value
S_b	Rated output power	5 MVA
V_b	Rated voltage	690 V
n_p	pole pairs	4
ω_B	Base angular electrical frequency	$100\times\pi$ rad/sec
J_g	Generator moment of inertia	2.12×10^6 kgm^2
R_s	Stator resistance	8.28×10^{-4} Ω
L_s	Stator inductance	4.091×10^{-5} H
ψ_{pm}	Permanent magnet flux linkage	1.7036 Wb